Multi-omics analysis of severe fever with thrombocytopenia syndrome virus infection in Rhipicephalus microplus cells reveals antiviral tick factors.

Marine Petit
m.petit@surrey.ac.uk
University of Surrey https://orcid.org/0000-0001-7427-7203
Charlotte Flory
Leibniz Institute of Virology
Quan Gu
MRC-University of Glasgow Centre for Virus Research https://orcid.org/0000-0002-1201-6734
Mazigh Fares
Medical Research Council–University of Glasgow Centre for Virus Research
Kelsey Davies
MRC-University of Glasgow Centre for Virus Research
Alan Score
Fingerprints Proteomics Facility, School of Life Science, University of Dundee
Douglas Lamont
Univesity of Dundee
Lesley Bell- Sakyi
University of Liverpool
Pietro Scaturro
Leibniz Institute of Virology https://orcid.org/0000-0001-9098-3087
Benjamin Brennan
MRC-University of Glasgow Centre for Virus Research https://orcid.org/0000-0003-4707-726X
Alain Kohl
Liverpool School of Tropical Medicine

Article

Keywords:

Posted Date: June 13th, 2024

DOI: https://doi.org/10.21203/rs.3.rs-4505289/v1

Additional Declarations: There is **NO** Competing Interest.

Abstract

The increasing prevalence of tick-borne arboviral infections worldwide necessitates advanced control strategies, particularly those targeting vectors, to mitigate the disease burden. However, the cellular interactions between arboviruses and ticks, especially for negative-strand RNA viruses, remain largely unexplored. Here, we employed a proteomics informed by transcriptomics approach to elucidate the cellular response of the Rhipicephalus microplus-derived BME/CTVM6 cell line to severe fever with thrombocytopenia syndrome virus (SFTSV) infection. We generated the first de novo transcriptomes and proteomes of SFTSV- and mock-infected tick cells, identifying key host responses and regulatory pathways. Additionally, interactome analysis of the viral nucleoprotein (N) integrated host responses with viral replication mechanisms. Finally, our dsRNA-mediated gene silencing screen revealed two novel anti-SFTSV effectors, the RNA helicases, DHX9 and UPF1. Collectively, our results provide new insights into the antiviral responses of Rhipicephalus microplus vector cells and highlight critical SFTSV restriction factors, while enriching transcriptomic and proteomic resources for future research.

Introduction

Severe fever with thrombocytopenia syndrome virus (SFTSV) (*Dabie bandavirus*, *Phenuiviridae, Bunyavirales*) is a tick-borne bunyavirus first discovered in China in 2009[1]. The human case fatality rate is around 10%, though this may vary by strain[2], with patients developing a range of symptoms including fever, leukocytopenia, thrombocytopenia, and gastrointestinal symptoms[3]. The virus has been detected in China[1], South Korea[4], Japan[5], Taiwan[6], and Vietnam[7], demonstrating a wide geographic distribution. There is an increasing understanding of the human immune responses to infection, immunopathogenesis, and viral counteraction of immune responses (mediated through the activity of the SFTSV non-structural [NSs] protein) during infection, but currently there are no specific antiviral treatments or vaccines available to threat this disease[8, 9, 10, 11].

The genome of SFTSV resembles that of related bunyaviruses, with the L segment encoding the RNA-dependent RNA polymerase (L); the M segment encoding a polyprotein precursor of the viral glycoproteins; and the S segment encoding the nucleoprotein (N) and the NSs protein which is a virulence factor and interferon antagonist in vertebrate infections. The genome termini interact to give a characteristic panhandle structure to the viral ribonucleoprotein complexes, in which the N protein encapsidates the viral genomic or antigenomic sense RNA. Both L and N proteins are critical for viral replication and transcription, however the host factors that regulate these processes during *Phenuivirus* infection in tick cells remain elusive[12, 13].

SFTSV is likely transmitted by several tick species including *Haemaphysalis (H.) longicornis*[14], *H. flava*[15], and *R. microplus*[6] to human or other vertebrate hosts. The molecular interactions between ticks and tick-borne arboviruses are poorly understood in particular the interactions of negative-sense RNA viruses, such as bunyaviruses for which most work has been conducted in vertebrate cell lines[16]. The virus-vector interactions are likely to influence virus transmission from the vector to vertebrate hosts, therefore, a deeper understanding is critical from virological, biological, and translational angles.

Tick cells respond to microorganisms and viruses with a range of cellular and immune responses[17, 18], but studies of tick-pathogen interactions at the molecular level are limited, particularly outside the genus *Ixodes*. Published studies have largely focused on tick-borne flaviviruses, such as investigations into the role of RNA interference (RNAi) in arbovirus-tick interactions in *Ixodes* spp.[19, 20, 21]. Critically, these studies also described the impact of virus infection on the metabolic, stress and nucleic acid metabolism pathways within the tick cell[20, 22, 23]. Recently, induction of RNAi responses by SFTSV and a potential role for SFTSV NSs as an RNAi suppressor were described during experimental infection of whole *H. longicornis* ticks[24]. That study also demonstrated that SFTSV infection affects metabolic processes, including the Toll pathway, although no functional analysis was performed, showing the considerable gaps in connecting transcriptome data with cellular effects, such as physiological or immunological impacts following infection.

Here we investigated the interaction of SFTSV with cells derived from a natural vector (*R. microplus*) by using a proteomics informed by transcriptomics (PIT) approach to investigate tick protein expression in response to SFTSV infection, exploring the cellular processes beyond the transcriptomic level. We combined the novel genomic and proteomic information we obtained from SFTSV-infected tick cells to assess the interactome of the SFTSV N protein and we selected nine targets for further characterisation. Notably, two RNA helicase proteins were identified as novel SFTSV restriction factors: the mRNA decay effector Up-Frameshift 1 (UPF1) protein, a key component of the nonsense-mediated mRNA decay (NMD) pathway[25]; and the multifunctional RNA helicase DHX9, which plays critical roles in various cellular processes, including the NF-κB antiviral response in vertebrate cells[26]. The identification of these two RNA-binding proteins as SFTSV antagonists represents a significant advancement in our understanding of the molecular mechanisms underlying tick-borne bunyavirus-vector cell interactions.

The transcriptome and proteome of *R. microplus* cells.

Given the limited understanding of tick cell biology, it is of considerable difficult to study how SFTSV hijacks and re-wires vector cells to establish infection. Therefore, we aimed to establish a novel study system to investigate SFTSV-tick cell interactions in the *R. microplus* cell line, BME6[27, 28]. BME6 cells, when infected with SFTSV at a MOI of 1 PFU/cell, reached an infection rate of approximately 60% by 3 d.p.i., indicative of the early viral expansion phase, and increased to 90% by 6 d.p.i., a late stage at which we also observed a 10-fold increase in viral titre, demonstrating the temporal dynamics of the infection (Fig. 1a,b). To examine how virus infection impacts BME6 cell biology we implemented PIT methodology, facilitating the integration of paired proteomic and transcriptomic data to generate the first comprehensive datasets for SFTSV infection in BME6 cells (Fig. 1c).

To generate the mock- or SFTSV-infected BME6 cell transcriptome, we employed a ribosomal RNA (rRNA) depletion protocol as described by Fauver et *al.* 2019[29]. We designed customed probes specific to *R. microplus* rRNAs resulting in their minimal detection in our sequencing. This allowed for the sequencing of a wide array of RNA species including non-coding RNAs (ncRNAs), viral RNAs, and mRNAs, from mock and SFTSV-infected tick cells, thereby providing a complete view of the transcriptional alterations induced by SFTSV infection. Transcripts sequenced from BME6 cells were assembled *de novo* using sequence reads, from mock and 3 d.p.i. samples, in Trinity[30] (Supplementary Table 2). This BME6 *de novo* transcriptome was then translated into six open reading frames (ORFs) to construct the protein search database for proteomic analysis, retaining ORFs longer than 66 amino acids and incorporating all SFTSV proteins listed in the Uniprot database. We identified 7511 unique protein groups, with 4750 of these groups confirmed by the presence of six or more peptides, using the PIT-predicted spectra as the search database for mass-spectrometry analysis (Supplementary Table 3, Supplementary File 1).

The current genome annotations of *R. microplus* are based on whole ticks or saliva analysis, therefore we decided to generate a genome annotation specific to our BME6 cells. *De novo* assembled transcriptome and proteome data underwent multiple search strategies including BLAST search[31], ortholog search (EggNOG[32], KEGG[33]) and protein domain search (InterProscan)[34, 35] to identify and annotate transcripts and proteins. Among the 29118 genes in the BME6 transcriptomes, 15660 were identified through BLAST searches, and 1207 through ortholog searches (Fig. 1d, Supplementary Table 2). Remaining contigs were either reported as transposable elements, or gene loci with no specified function or structure that we designated as uncharacterized, requiring further investigation to establish their function or gene structure i.e ncRNAs. Our annotation pipeline resulted in the annotation of 92% of the BME6 proteins identified (Fig. 1e). Tick-specific viral transcripts and proteins, including the complete genome of Wuhan tick virus 2 (*Chuviridae*)[36] and the IRE/CTVM19-Rhabdovirus, were identified in the BME6 cells used in our study[37, 38].

Finally, we used the Program to Assemble Spliced Alignments (PASA) software in conjunction with the EVIdenceModeler (EVM)[39] program to facilitate the identification of new BME6-derived genes and novel spliced alignments. Of our 29118 PASA-EVM identified genes, 8000 presented novel alternative splicing events (Fig. 1f, Supplementary Database). Identification of novel gene candidates and previously unidentified splicing events took multiple forms such as expansion of existing ORFS, new splicing pattern, or new transcripts variants (Fig. 1g). These demonstrate the value of PIT analysis regarding the study of organisms with poor genome annotations such as the tick species *R. microplus*. The overall improvement of gene, transcript and protein information obtained by our approach critically enhances our understanding of SFTSV infection of these vector cells[40] (Extended Data Fig. 1), as outlined further below.

SFTSV infection affects temporal BME6 cellular transcription and protein abundance.

To elucidate the impact of SFTSV infection on tick cells, we performed a comparative analysis of mock and SFTSV-infected BME6 cells at both the transcriptome and proteome levels. RNA sequencing reads were mapped back to the Trinity generated *de novo* transcriptome using STAR aligner[41] (Fig. 1). Analysis revealed an increase in the number of differentially regulated transcripts at 3 d.p.i. in the SFTSV-infected BME6 cells compared to the mock-infected control. This difference was even more pronounced at the later time point of 6 d.p.i. (Fig. 2a,b). While 193 up-regulated and 18 down-regulated transcripts were common to both early and late infection time points, the majority of differentially expressed transcripts were unique to each time point (Fig. 2c), suggesting time-dependent viral impact of the cellular RNA pool. We next analysed BME6 protein alterations using our newly annotated proteome (Fig. 1). We examined proteins that were differentially regulated at either 3 or 6 d.p.i. relative to mock-infected control cells. Our comparison uncovered distinct protein abundance profiles in response to SFTSV infection at 3 and 6 d.p.i. As in our transcriptome analysis, minimal changes were observed at 3 d.p.i. (Fig. 2d) compared to a significant shift evident at 6 d.p.i., where 387 proteins were downregulated, and 1238 proteins were upregulated (Fig. 2e). 59 and 3 proteins were, respectively, significantly up- or down-regulated at both time points (Fig. 2f). Finally, 776 proteins up-regulated and 37 proteins down-regulated proteins were unique to 6 d.p.i., indicating a temporal response to SFTSV. These observations suggest that the timing of SFTSV replication kinetics differently affects the dynamics of protein levels in infected tick cells.

To investigate the effects of SFTSV infection on post-transcriptional regulation in BME6 cells we analysed the relationship between RNA transcripts levels and protein abundance. The Pearson correlation coefficient was used to evaluate the association between 4559 previously identified proteins and their related transcripts. At 3 d.p.i., we observed a modest positive correlation of 0.28 (Fig. 2g), suggesting a low but

nevertheless significant relationship between RNA and protein levels. We found 2 k-means clusters comprising transcript-protein pairs with a strong correlation. This may indicate that various factors influence protein levels beyond transcript abundance. This trend was accentuated at 6 d.p.i. with a correlation factor of 0.12 (Fig. 2h), suggesting that SFTSV infection changes post-transcriptional and translational processes. Most antiviral genes (identified in previous studies) that were significantly up- or down- regulated in our transcriptomics and proteomics analysis (HSP68, Trypsin-1, XIAP-like, Microplusin) were not included in the k-means clusters, pointing to distinct regulatory mechanisms for these genes. Altogether our results indicated a complex regulatory landscape governing gene expression and protein biosynthesis in tick cells when infected with SFTSV.

SFTSV infection regulates BME6 cell immune- and stress-related pathways.

To further characterize biological processes altered during SFTSV infection we ran a pathway analysis, using the recently described *R. microplus* ensemble metazoa gene ontology (GO) categories[40]. Subsequent GO analysis of annotated transcripts and proteins revealed limited alterations at 3 d.p.i. but significant upregulation of various GO categories at 6 d.p.i. (Extended Data Fig. 2). For both time points we observed SFTSV-mediated down-regulation of oxidoreductase activity and protein binding categories (i.e., HSP70-interacting protein, NF-κB modulator); and the up-regulation of RNA-dependent RNA polymerase activity, a category associated with the synthesis of small and non-coding RNA in ticks[42]. However most enriched GO categories were time-dependent, validating our previous observation at the transcriptome, and proteome levels (Extended Data Fig. 2). Although pathways linked to innate immunity or antiviral responses were not identified, the possibility that insufficient genome annotations and GO categorizations contributed to this finding cannot be dismissed.

To broaden our understanding of the antiviral responses against SFTSV infection and to identify the BME6 cell core immune pathways, we combined previously identified tick-derived immune effectors[20, 23, 43] with our newly annotated proteome. Through characterization of the IMD, Toll, JAK-STAT, and JNK pathways (summarised in Fig. 3a), we observed a moderate up-regulation of these signalling cascades at 6 d.p.i. as well as of several pattern recognition receptors including the IMD pathway receptor Croquemort[44] and the cytokine receptor Domeless-like (Fig. 3b). Further antiviral effectors related to arthropod antiviral responses were identified including heat shock factors[45], and tick-specific antimicrobial effectors such as Microplusin and Galectin[46], which were up-regulated during SFTSV infection (Fig. 3a). Additionally, key components of the RNAi pathway, including Dcr2, Ago2, and Loquacious, were also identified. However, no significant regulation of these RNAi proteins was observed during SFTSV infection. We next examined the expression profiles of the MAPK pathways, where all effectors were identified but only the receptor RTK, and downstream factors such as MKNK1 and MPK2, were significantly up-regulated at 6 d.p.i. (Fig. 3b). These data suggest that *R. microplus* MAPK pathways are not involved in the response to SFTSV infection.

As our transcriptome analysis identified SFTSV regulation of stress-related genes during BME6 cell infection e.g. TP53 or calpain-A-like, we decided to extend our characterization to examine differential expression of the apoptosis and mitochondrial stress pathways. Expression of apoptosis effectors, such as APAF1, Bax-1, and p53, was not changed during SFTSV infection, while expression of apoptosis inhibitors including XIAP or Bcl2-like was significantly up-regulated at 6 d.p.i., suggesting inhibition of apoptotic processes during SFTSV infection. A similar trend was observed for mitochondrial stress effectors and DEAD box RNA helicases including two anti-bunyaviral candidates identified previously in mammalian cells, DDX17 and DDX51[47, 48] (Fig. 3b). Altogether our analysis describes the first comprehensive examination of temporal proteome and transcriptome level changes in tick cell genes induced by SFTSV infection of *R. microplus*-derived cell cultures.

SFTSV nucleocapsid protein co-opts stress pathways in both early and late infection.

To further elucidate the intricate interplay between SFTSV and BME6 cells, we investigated the SFTSV N protein interactome with *R. microplus*-derived cells. SFTSV N antibody[49] was used to immunoprecipitate cellular proteins interacting with the viral nucleocapsid protein N during infection. α-Tubulin immunoprecipitation served as a control. Immunoprecipitated extracts were derived from mock and SFTSV-infected BME6 cell cultures at 3 or 6 d.p.i. and subjected to analysis by mass spectrometry (Fig. 4a). The N interactome data were standardised to control conditions, e.g., anti-N immunoprecipitated lysates from mock-infected cells and anti-tubulin immunoprecipitated lysates from infected cells were examined as a cross comparison to discard non-specific interactors. We identified 16 proteins interacting specifically with SFTSV N at 3 d.p.i., 44 proteins specifically interacting at 6 d.p.i. and 22 common to both time points (Fig. 4b, Supplementary Table 4). Importantly, our data also determined the expected interaction between the viral N and L proteins. We also confirmed interactions of SFTSV N with the cleavage and polyadenylation specificity factor subunit 6 (CPSF6) and the insulin-like growth factor 2 mRNA-binding protein 1 (IGF2BP1) (Fig. 4b) as previously observed in mammalian cell lines[64]. Several of our newly identified N protein interactors have been previously classified as antiviral effectors, all of which are involved in the NF-κB response to arboviral infection in vertebrate cells, including the Toll receptor associated factor 2 (TRAF2), the NF-κB restriction factor (NκRF) and the DExD/box helicase DHX9[50]. Finally, corroborating our observations on transcriptome and proteome changes, we identified interactions between SFTSV N and key mitochondrial stress factors, as well as proteins associated with stress granules, including a novel interaction between SFTSV N and Up-frameshift protein 1 (UPF1) which is essential to the non-sense mRNA mediated-decay (NMD)

pathway[51] (Fig. 4b). Using a KEGG pathway analysis we were able to assign the remaining SFTSV N interactor to the spliceosome, glycolysis, or mRNA surveillance pathways (Fig. 4c). Finally, to understand if uncharacterized proteins were associated with the identified pathways, we performed a protein domain search analysis using InterProScan[35]. Of the nine uncharacterized proteins, seven were associated with functional domains including tautomerase and transglycosylase domains, RNA recognition motifs, or domains derived from transposable elements (e.g retrotrans_gag) (Fig. 4d, Supplementary Table 5).

Restriction of SFTSV infection by antiviral, and stress effectors in BME6 cells.

The identification of differentially regulated transcripts and proteins, as well as N protein interactors in SFTSV-infected BME6 cells alone does not demonstrate biological significance. To address this, we conducted knockdown of targeted transcripts in BME6 cells; given our identification of the siRNA pathway components in the BME6 cell line (Fig. 4b), this was achieved through gene silencing using transfection of dsRNA targeting host genes (Fig. 5a).

As transfection of the BME6 cell line had not been previously documented, we identified O2 Magnetofection technology (Oz Bioscience) as the best option to deliver target dsRNAs linked to magnetic beads into cells, using a magnetic field (Extended Data Fig. 5). Magnetofection efficiency was assessed, using dsRNA targeting the SFTSV N protein (Table 1). At 18h post-dsRNA transfection, BME6 cells were infected with SFTSV at a MOI of 0.5 PFU/cell. Samples collected at 3 and 6 d.p.i. showed a reduction of SFTSV RNA copy number in infected cells as determined by RT-qPCR of the M segment (Fig. 5c) and number of infectious virus particles, assessed by plaque assay (Fig. 5d). This suggests that transfection of dsRNA targeting SFTSV N could efficiently knockdown expression of this protein in SFTSV-infected tick cells.

We next used dsRNA to knock-down and identify selected targets as SFTSV restriction factors in BME6 cells, in partcular those associated with antimicrobial functions or that were significantly up-regulated in our transcriptomics/proteomics analyses. These included: HSP68 and Microplusin from transcriptomic data; Croquemort and SCARB1 from proteomics analysis; and DHX9, PAPB4, TRAF2, SMF7, and UPF1 from our N interactomics dataset. For each target we designed ~500 nt specific dsRNAs (Table 1) that were transfected into BME6 cells at 18 h prior to SFTSV infection. Target silencing was generally effective, though for some transcripts variation or absence of silencing were observed (Fig. 5d1-g1). No significant differences were seen with regards to an impact of target silencing on viral M segment RNA, except for DHX9 at 6 d.p.i. (Fig. 5g1-g3). Silencing of certain host factors, such as HSP68 and the antimicrobial peptide Microplusin appeared to restrict virus production early on (Fig. 5d3), while targeting the N interactor DHX9, restricted SFTSV virus production at both 3 and 6 d.p.i., suggesting a constant role for this RNA-helicase A during the viral infection (Fig. 5f3). Finally, we sought to determine if NMD pathway-SFTSV interactions identified from our N interactome studies, impacted SFTSV replication (Fig. 5g1-g3). UPF1 and SMG7, both NMD effectors and identified as N interactors[51] (Fig. 4), were successfully knocked down, except for UPF1 at 3 d.p.i. (Fig. 5h1). SFTSV M segment RNA levels were unchanged at 3 d.p.i. but increased significantly at day 6 p.i. when UPF1 transcript expression was ablated (Fig. 5h2); this increase was also observed for viral titres, suggesting that UPF1 but not SMG7 restricted SFTSV infection in tick cells (Fig. 5h3). Interestingly, *R. microplus* UPF1 is closely related to human UPF1, suggesting potentially similar function(s) in tick and human cells (Extended Data Fig. 5).

Discussion

Our study provides the first multi-omics analysis of tick cells infected by a tick-borne bunyavirus. Through PIT analysis of SFTSV-infected *R. microplus* cells, we provide the first integrated transcriptomic and proteomic profiles of BME6 cells (Fig. 1). Facilitating the characterization of several mRNAs/isoforms, alongside the identification of 386 novel proteins annotations, our study advances our comprehension of the genomic and proteomic complexity of *R. microplus* BME6 cells. By focusing on the cellular response to SFTSV infection our data demonstrated the conservation and function of various of antiviral mechanisms, including innate immune pathways, stress related pathways and mRNA surveillance mechanisms (Fig. 2-3). The integration of this improved understanding of tick cell biology with methodologies such as AP-MS and dsRNA knock-down screening has enabled the discovery of novel viral restriction factors such as the RNA helicases UPF1, and DHX9 (Fig. 4-5). Our findings illustrated the dynamic changes of tick cells biology during viral infection and confirm the sophisticated nature of the arthropod innate immune response to viral infection[52].

Previous work has used *Ixodes* species to study the antiviral mechanisms present in tick cell lines, but there have been few efforts to use a negative sense RNA virus-tick model as observed in nature. Only a recent study has used a non-*Ixodes* tick to characterize the RNAi response to viral infection[53]. Here we developed a *R. microplus* BME6 cell-based model associated with a systems biology approach[54] to obtain a detailed understanding of SFTSV-tick cell interactions. The generation of a BME6 cell *de novo* transcriptome and proteome was central to the characterization of these processes. By associating PASA-EVM and ortholog annotations, we joined the collective effort to complete the *R. microplus* genome and proteome to support understanding of the tick-SFTSV co-evolution[17, 55].

Additionally, our rRNA depletion protocol allowed us to identify the regulation of numerous unannotated transcripts, indicative of an expanded ncRNAs repertoire in *R. microplus*. Although the detection of ncRNAs is now standard, their functional roles, particularly in the context of viral

infection, are not well characterized[56, 57]. For instance, during vertebrate host infections with vector-borne pathogens, ncRNAs have been identified that either indirectly regulate translation via miRNAs or directly through long-ncRNAs[58]. This mechanism could account for the observed low correlation between mRNA and protein levels in our datasets at 6 d.p.i. as shown in Figure 3. Further research is essential to elucidate the specific roles of ncRNAs in virus-infected tick cells[59, 60].

With our systems virology approach, we improved the characterization of major innate immune pathways of *R. microplus* including JNK, JAK-STAT, Toll and Imd pathways which were also identified in *I. scapularis*, showing a high level of conservation across ixodid ticks[40, 46]. However, their role in the tick antiviral response remains unclear. While we identified some factors common to tick-borne flavivirus[19, 20] and tick-borne bunyavirus infections, such as the upregulation of trypsin at days 3 and 6 p.i. and the regulation of complement H factor or SCARB1 (CD36) receptor, better genome annotation and methodologies are still needed to comprehensively identify pan-antiviral effectors across the different virus families[20, 23]. Importantly RNAi serves as a fundamental defence mechanism in arthropods[19]. Our study not only identified RNAi effectors, but also leveraged RNAi to facilitate dsRNA-mediated knock-down in tick cells (Fig. 5). Beyond the canonical RNAi components, including Dcr2 and Ago2, our multi-omics analysis also revealed the expression of Dcr1, Ago3 and Aub proteins from the miRNA and piRNA pathways. Further investigations should indicate if, similarly to mosquito cells, tick cells involve for example the piRNA in antiviral responses[61].

Our datasets, as well as previous studies utilising flavivirus infections have shown the presence and regulation of various tick cellular stress factors in response to infection[20, 21, 23, 62]. Indeed, flavivirus-infected *I. scapularis* cells demonstrated regulation of apoptosis through regulation of pro-apoptotic factors like bcl2, and metabolic effectors linked to the stress responses, including oxidative stresses[21]. These processes would appear to confer beneficial impact to the virus, enhancing replication. This shows that both positive and negative sense RNA viruses can interact with cell stress pathways during tick cell infection.

Importantly, we identified for the first time an interaction between mRNA surveillance factor UPF1 and the SFTSV N protein in infected cells. Moreover, restriction of SFTSV replication by UPF1 showed that this RNA helicase regulates SFTSV replication. While we provide the first evidence of UPF1 antagonism of a bunyavirus in an animal cell, the mechanism involved remains unclear. UPF1 could degrade viral RNAs *via* its RNA helicase function conserved in both NMD and the alternative Staufen mRNA decay mediated (SMD) pathways[51, 63] (Extended Data Fig. 5). Alternatively, the role of UPF1 in stress granules formation may help sequestrate cellular 5' caps essential for bunyavirus replication, as described for plant-infecting bunyaviruses[64]. The involvement of the NMD pathway in cap-snatching regulation was supported by a second study linking hantavirus N protein, decapping enzyme, and stress granules[65]. This last hypothesis would explain the identification of several proteins related to stress granule formation in our N interactome datasets (Fig. 5).

Another RNA helicase, DHX9, displayed a consistent restriction of SFTSV infection in BME6 cells (Fig. 5). DHX9 emerges as a multifaceted helicase with pivotal roles in RNA regulation and nucleic acid recognition, exhibiting both pro-viral and anti-viral activities within vertebrate systems[66]. DHX9 is characterized by its dual nucleic acid recognition domains: one domain is specific for DNA, which facilitates pro-viral activities, notably in the context of HIV-1[67] and herpesviruses[68]. The second recognition domain of DHX9 targets dsRNA and showed anti-viral function against two alphaviruses, Chikungunya and Sindbis, for which recruitment of DHX9 to viral replication complexes negatively impacted viral RNA synthesis[69, 70]. Although DHX9 has an established antiviral function against RNA viruses in arthropods[71], our investigation has revealed the first instance of DHX9 exerting a restrictive activity against a negative-sense RNA virus in arthropod cells. This novel finding expands our understanding the antiviral spectrum of DHX9. However, it also underscores the necessity for additional studies to fully decipher the mechanisms underlying the action of DHX9 in this context.

In conclusion, this in depth study significantly advances the understanding of tick cell biology and antiviral mechanisms through a comprehensive multi-omics analysis. With the identification of novel vector cell antiviral restriction factors, UPF1 and DHX9, we demonstrate the suitability of PIT for functional studies of less well-characterized organisms such the tick vector *R. microplus*.

Materials and Methods

Cells and virus. Cells of the *R. microplus* cell line BME/CTVM6 (BME6), obtained from the Tick Cell Biobank, were grown in L-15 medium supplemented with 20% foetal bovine serum (FBS) and 10% tryptose phosphate broth (TBP) at 28 °C as previously described[28]. Tick cells were grown in 3 ml volumes in sealed, flat-sided tubes (Nunc, Fisher Scientific, UK), with weekly medium changes and subculture at intervals of 2 weeks. Vero E6 cells were obtained from Michle Bouloy (Institut Pasteur, France) and grown in Dulbecco's modified Eagle's medium (DMEM) supplemented with 10% FBS, at 37 °C, in an atmosphere of 5% CO2 in air. The SFTSV strain used in this study was a plaque-purified, cell culture-adapted stock called Hubei 29pp (HB29pp) provided by Amy Lambert (CDC Arbovirus Diseases Branch, Division of Vector-Borne Infectious Diseases, Fort Collins, CO, USA)[72]. Working stocks of SFTSV were generated in the Vero E6 cell line by infecting at a low multiplicity of infection (MOI) and harvesting the cell culture medium 7 days post infection (d.p.i.). Experiments with SFTSV were performed under containment level 3 conditions, approved by the UK Health and Safety Executive.

Virus infection and plaque assay. BME6 cells were seeded in 12 cm^2 non-vented flasks with a density of 310^6 cells per flask with 4 ml of L-15 medium. For the proteomics informed by transcriptomics (PIT) experiments, BME6 cells were inoculated with SFTSV at a MOI of 1 PFU/cell, and samples (supernatants and cell lysates) were collected at 3 d.p.i. For the differential gene and protein expression analyses we added a supplementary time point at 6 d.p.i. Regarding biological validation experiments, target knock down (KD) and parental BME6 cells were infected with SFTSV at a MOI of 0.5 PFU/cell, samples (supernatants and cell lysates) were collected at 3- or 6- d.p.i. For all experiments, virus titres in samples were determined by plaque assay in Vero E6 cells. Briefly, confluent monolayers of Vero E6 cells were infected with serial dilutions of virus made in phosphate buffer saline (PBS) containing 2% FBS and incubated for 1 h at 37 °C, followed by the addition of a Glasgow MEM overlay supplemented with 2% FBS and 0.6% Avicel (FMC Biopolymer). Cells were then incubated for 6 days before fixation (4% formaldehyde) and staining with methylene blue to visualize viral plaques.

RNA and protein purification from BME6 cells. Approximately 310^6 SFTSV- or mock-treated BME6 cells were scraped into L-15 medium, harvested by centrifugation (100 x g, 10 mins, 4 °C), washed twice with ice-cold PBS and divided into two samples which were then used for either RNA or protein extraction. For RNA isolation, the cell pellet was resuspended in 1 ml of TRIzol® reagent (ThermoFisher Scientific) and purified as described by the manufacturer. For protein isolation, the samples were resuspended in 100 µl of lysis buffer (4% NP-40, 10 mM Tris (2-craboxyethyl) phosphine (TCEP) and 50 mM triethylammonium bicarbonate (TEAB)).

rRNA depletion, RNA sequencing and analysis. To perform rRNA depletion of the samples, we modified the Fauver et *al.* 2019[29] protocols to fit the peculiarities of *R. microplus* tick ribosomal RNAs. Briefly, we performed nucleic acid extraction using TRIzol® reagent (ThermoFisher Scientific) following the manufacturer's instructions. The samples were then treated with TURBO DNase (ThermoFisher) and purified using RNAClean XP beads (Beckman Coulter). For reverse transcription, the RNA was combined with rRNA specific oligonucleotides (sequences listed in Supplementary Table 1) and dNTPs. Samples were then heat-denatured at 95 °C for 2 min, followed by slow cooling to 50°C at a rate of 0.1 C/s. Avian myeloblastosis virus reverse transcriptase (AMV, NEB) was added to samples and incubated at 50 °C for 2 h. Subsequently, RNase H (NEB) and DNaseI treatment was introduced to eliminate the RNA from the resultant RNA:cDNA hybrid and the residual oligonucleotides. The resulting RNA was concentrated and purified using the RNA clean & concentrator-5 kit (Zymo Research). Input and rRNA-depleted RNA were analysed using a 2100 Bioanalyzer (Agilent) per manufacturer's protocols with the total RNA Pico kit. BME6 rRNA depleted RNA samples were sent to Azenta Genewiz for a standard RNA-sequencing library preparation (no fragmentation, no enrichment) and sequencing using Illumina NovaSeq 2x150 bp sequencing. Following sequence filtering and trimming ~60 million paired end reads were obtained for our 12 samples. The quality of all reads was evaluated using FastQC (v0.11.5, https://www.bioinformatics.babraham.ac.uk/projects/fastqc/). The Trinity *de novo* assembly software (v2.14.0)[30], was used to produce a set of assembled transcripts from the RNA-seq data (~2.83 million contigs) using the default parameters.

DIA proteomics. Following cell lysis, the protein were resuspended in S-trap binding buffer (90% aqueous methanol containing a final concentration of 100 mM TEAB, pH 7.1), then quantity was measured by micro-BCA assay. Identical amounts of proteins were prepared and loaded in the S-trap column where proteins are captured within the submicron pores of the three-dimensional trap. Standard S-Trap protocol for mini columns was used but number of washes were increased to 10. The digesting buffer containing trypsin was added to the S-trap column. After 12h trypsin digestion followed by a second 6h trypsin treatment, peptides were eluated in a 50 mM TEAB solution. Dried peptides were resuspended in 0.1% formic acid before quantitative fluorometric peptide assay. 1.5 µg of peptides were loaded into an Orbitrap Exploris 480 MS. The DIA analysis was performed on Spectronaut (version 16.2.220903.5300) using a custom 6-frame translated database generated from the transcriptomic dataset. Proteomics were performed by the FingerPrints Proteomics Facilities at the University of Dundee, UK.

Proteomics informed by transcriptomics analysis (PIT). Files from the DIA MS/MS analysis were first converted to mzML files using Proteowizard[73] whilst the *de novo* transcriptome produced by Trinity software (containing ~2.8M contigs) was translated in to all six open reading frames (ORFs with a start codon and > 66 amino acids) using Transdecoder software (Haas, BJ. https://github.com/TransDecoder/TransDecoder) to produce ~6.8 million ORFs. The resultant FASTA files were used in a database search and subsequent protein annotation pipeline. Carbamidomethyl was chosen as a fixed modification, and N-terminal acetylation, asparagine/glutamine deamidation, methionine oxidation or dioxidation, and conversion of glutamine to pyro-glutamic acid as our variable modifications. Searches were performed with full tryptic digestion and using the following parameters max peptide length 52, min. peptide length 7, missed cleavages 2, m/z max. 1800 min 300. Spectronaut default settings were modified with decoy generation set to inverse; Protein LFQ Method was set to QUANT 2.0 (SN Standard) and data filtering to qvalue; precursor qvalue cutoff and protein Qvalue Cutoff set to 0.01, precursor PEP cutoff set to 0.1 and protein qvalue cutoff (Run) set to 0.05. Major Group Top N, Minor Group Top N and Cross-Run Normalization were not selected. PSM-peptides-proteins FDR of 0.01. This allowed the identification of ~150000 peptides corresponding to Trinity-generated transcript ORFs. The transcripts were mapped to the Trinity files containing

all the transcripts using the aligner STAR[41]. The identified transcriptomic and proteomic features were then combined into a single file. In the final step of the workflow, we used diamond BLASTX[74] to compare each protein sequence against the *R. microplus* genome[40] (NCBI-RefSeq: GCF_013339725.1) and the NCBI non-redundant database. To increase the annotation of the remaining non-annotated protein sequences, we used the eggNOG 4.5 algorithm[32] for ortholog identification and InterProScan 5 search[34] to identify SUPERFAMILY or Pfam motifs to allow for protein domain annotation. Whilst mock and 3 d.p.i. samples in 4 replicates were run in parallel, the 4 replicates for 6 d.p.i. samples were run independently.

-

Gene prediction. Genes were predicted on the RMIC2018 (*R. microplus* 2018*),* RefSeq genome with the PASA software system[75] (Program to Assemble Spliced Alignments v2.5.2) in conjunction with the EVidenceModeler (EVM) software v2.1.0[39]. We used Trinity *de novo* assembled transcripts, along with our *de novo* PIT proteome as input evidence for the PASA pipeline. Our PASA RNA-seq gene expression results were combined using EVidenceModeler to *ab initio* gene prediction (Augustus v3.5.0[76], SNAP[77]) and protein homology (exonerate v2.4.0[78], miniprot v0.12[79], genome threader[80]). We used the following weighted consensus: *ab initio* prediction assigned value of 1, protein alignment assigned value of 2, Pasa transcript assemblies assigned value of 10. EVidenceModeler software produced a set of 29118 gene models and 8000 novel splicing events, all disclosed in our SQLite PASA-EVM database.

Differential gene expression analysis. rRNA-depleted RNA reads were mapped against our *de novo* transcriptome with STAR (v2.5.2b)[41]. HTseq (v0.6.1) was used to count all reads for each transcripts and set up a read count table[81]. Differential gene expression analyses were performed using the DESeq2 Bioconductor package (v1.30.1)[82]. The default "normal" shrinkage (v1.28.0)[83] set up was used for analysis. Gene-ontology analysis was performed with the g:Profiler website[84] using the data Ensembl Metazoa Rmic18[40].

Differential protein expression analysis. The Perseus software v.1.6.15.0 was used to further process the DIA proteomics datasets. Protein tables were filtered to eliminate the identifications from the reverse database and common contaminants. In the subsequent MS data analysis, only proteins identified based on at least six peptide and a minimum of three quantitation events in at least one experimental group were considered. The protein intensity values of the interactome dataset were log2-transformed, missing values were filled by imputation with random numbers drawn from a normal distribution calculated for each sample[85]. Results were presented in Volcano plots.

Affinity purification and mass spectrometry (AP-MS) of SFTSV N protein. BME6 cells were infected with SFTSV HB29 at a MOI of 1 PFU/cell (310^6 cells per $12cm^2$ flask) and harvested at 3 or 6 d.p.i. by scraping cells into 1 ml of lysis buffer (50 mM Tris (pH 8), 150 mM NaCl, 0.5% NP-40, cOmplete protease inhibitor cocktail, Roche). SFTSV N-affinity purifications (AP) were adapted from the previously described AP-MS protocol for Zika virus proteins by Scaturro and colleagues[86]. In brief, clarified cell lysates were incubated with anti-N-coated beads at 4 °C, and non-specifically bound proteins were removed by three washes with lysis buffer and three washes with washing buffer (50 mM Tris (pH 8), 150 mM NaCl). Proteins were eluted in 2% SDS and PBS buffer. Eluted proteins were reduced and alkylated in 10 mM DTT and 55 mM iodoacetamide. The samples were acetone-precipitated twice and afterwards resuspended and denatured in 40 µL U/T buffer (6 M urea/2 M thiourea in 10 mM HEPES, pH 8.0) followed by digestion with 1 µg LysC (FUJIFILM Wako Chemicals) and 1 µg trypsin (Promega) in 40 mM ABC buffer (50 mM NH_4HCO_3 in water, pH 8.0) overnight at 25 °C, on a shaker at 800 rpm. Following digestion, peptides were purified on stage tips with 3 layers of C18 Empore filter discs (3M) as previously described[86]. Samples were analysed on a nanoElute (plug-in v.1.1.0.27; Bruker) coupled to a trapped ion mobility spectrometry quadrupole time of flight (timsTOF Pro) (Bruker) equipped with a CaptiveSpray source as previously described by Wanner, Andrieux and colleagues[87]. Raw MS data were processed with the MaxQuant software v.1.6.17.0 using the built-in label-free quantitation algorithm and Andromeda search engine[88]. The search was done against the *de novo* proteome from PIT analysis in this study (Supplementary File 1), and the Uniprot entry for SFTSV proteins. The Perseus software v.1.6.15.0 was used to further process the affinity-purification datasets. Protein tables were filtered to eliminate the identifications from the reverse database and common contaminants. In the subsequent MS data analysis, only proteins identified with at least one peptide and a minimum of three quantitation events in at least one experimental group were considered. The iBAQ protein intensity values of the interactome dataset were log2-transformed, missing values were filled by imputation with random numbers drawn from a normal distribution calculated for each sample[85]. Results were represented as a network using Cytoscape[89]. Mass-spectrometry was performed by the Systems Arbovirology team at the Leibniz Institute of Virology, Germany.

dsRNA production and transfection of *R.microplus* BME6 cells. RNA was extracted from BME6 cells using TRIzol® reagent (ThermoFisher Scientific) and reverse-transcribed using Superscript III Reverse Transcriptase (Invitrogen) following the manufacturer's instructions. PCR products were generated with T7 RNA polymerase promoter sequences at either end of the fragment using the primers listed in Table 1 and designated as for use *in vitro*. dsRNA was synthesized using the MEGAscript™ T7 Transcription Kit (Invitrogen) following the manufacturer's instructions. Synthesized dsRNAs were then transfected into BME6 cells to induce knock-down of the targeted genes**.** However, as BME6 cells are difficult to transfect by conventional methods, we used a magnetofection (MTX) kit for primary cells (02 Magnetofection, OZ Bioscience). Transfections were carried out in 6-well plates and 3 µg of dsRNA and 9 µL MTX transfection reagent were allowed to combine with 3 µg of magnetic nanoparticles (Combimag, Oz Biosciences) for 20 min. Nucleic acids were delivered into cells using a magnetic field on the top of the supplied magnetic plate for 30 min. Fresh medium was then added to the transfected cells which were then re-seeded in 12 cm^2 non-vented flask to allow for culturing.

Gene	5'	3'
Croquemort	**TAATACGACTCACTATAGGG**CAGCTTGGTCAAGGAGGGAG	**TAATACGACTCACTATAGGG**TTCGAGAAACGTGTAGGGGC
DHX9	**TAATACGACTCACTATAGGG**GCAAGTGGCTGTGGACAATG	**TAATACGACTCACTATAGGG**GCTTTAGTAGCCTCCCCACC
hsp68	**TAATACGACTCACTATAGGG**GTGCAAGAGTTCAAGCGGAA	**TAATACGACTCACTATAGGG**CCGTCTCGATGCCTAACGAC
Humanised *Renilla* Luciferase (control)	**TAATACGACTCACTATAGGG**GCGCCCTGGTTCCTGGAAC	**TAATACGACTCACTATAGGG**GAGAATCTCACGCAGGCAGTTC
Microplusin	**TAATACGACTCACTATAGGG**CTCACCACTTGGAGCTTTGC	**TAATACGACTCACTATAGGG**CAGCGTTGTGAATCTCCGTG
PAPB4	**TAATACGACTCACTATAGGG**AACATCCTGTCTTGTCGCGT	**TAATACGACTCACTATAGGG**ACAAGTTGACGCCCTGGTAG
SCARB1	**TAATACGACTCACTATAGGG**GGCATGAACCCAGATCCCAA	**TAATACGACTCACTATAGGG**GTTGCGCACTGCAGTAATCC
SMG7	**TAATACGACTCACTATAGGG**AGATTGGGATGTGCAGTGCT	**TAATACGACTCACTATAGGG**CAGAGCATCAGACGAGGGAC
TRAF2	**TAATACGACTCACTATAGGG**GACAAGGGCAGTTTCGAGGA	**TAATACGACTCACTATAGGG**GTAGTGTCCGGTCGGGAATG
UPF1	**TAATACGACTCACTATAGGG**TCTGCCCAAGCACTTCTCAG	**TAATACGACTCACTATAGGG**AACAGGCACCATACACTCCG

Table 1. Oligonucleotide sequences used to generate dsRNA. Oligos were designed based on genomic DNA sequences derived from BME/CTVM6 cells to generate the dsRNA necessary for RNAi-induced gene silencing. Bold sequences represent the T7 RNA polymerase promoter sequence used for *in vitro* RNA synthesis.

Quantitative reverse transcription-PCR (qRT-PCR). Total RNA of SFTSV-infected and mock-infected BME6 cells was isolated, at 3 and 6 d.p.i., using TRIzol reagent (ThermoFisher Scientific). cDNA was synthesized with SuperScript™ III reverse Transcriptase (Invitrogen). Real-time PCR was performed with iTaq SYBR Green premix (BioRad) and data were collected with QuantStudio 3 RT-PCR system (Thermo Fisher Scientific). All Ct values were normalized to the expression values of eif1A RNA and gene expression quantification were performed by the $2^{-\Delta\Delta Ct}$ method[90]. Oligonucleotide sequences utilised for qRT-PCR are provided in Table 2.

Gene	Forward	Reverse
Croquemort	TCATGGCTGGCACGGAAAA	CGGCTGGAAGTAGTATCGCT
DHX9	TTTGCCTTACCAGCAGGGAC	TGCAGCCTCGATTTTGCATT
eiF1A	CTCAGTGGTCAGGTTGGCAG	CGTCTACAAGATTGGCATT
HSP68-like	TCAATCCAGACGAGGCTGTT	GCCGTCTCGATGCCTAACG
microplusin	AAACTGAACTCCAGTGCATCG	ATGACGCAGCTCCTATCCCG
PABP-4	CGCCCGACCTACAAGTACAC	CCTGGAATGAAGCGGCAATG
SCARB1	TCCTACAAAGAGACCAAGCGT	TTCCTTTAGCAAATGCGCCG
SFTSV genome (M segment)	AGCCTTCTTCACGACAAGCA	TTCGTCATGGCTCAGGAACC
SMG7	CTCGACCTAGTCGCAAGCAT	CGCATATCTCGAGGGTCCTG
TRAF2	CAACACTGTTCTCAAGCGGC	TGGAGCATTTGTGTCACCGA
UPF1	TGATGAGGAACCCCAGCAAG	GTCTGCGACTCCTTCAGCTT

Table 2. Oligonucleotides used for RT-qPCR. List of the RT-qPCR oligonucleotides used for the quantification of host gene expression or viral RNA levels in tick cell cultures.

Immunostaining. Protein samples were resuspended in 4:1 NuPage:TCEP loading buffer, and heated for 10 min at 95 °C. Cell lysates were separated by SDS-PAGE on 4%-20% gradient polyacrylamide gels. Proteins were transferred onto PDVF 0.2 µm membrane (Hybond P, GE Healthcare). Membranes were blocked in 2% bovine serum albumin (Sigma A3059) in 0.1% TBS-Tween, then incubated overnight at 4 °C with mono-specific primary antibodies: rabbit anti SFTSV N^{72} and loading control anti α-tubulin ((#T5168, Sigma-Aldrich), both at a final dilution of 1:1000. Images were obtained on a LI-COR Odyssey CLX far red imaging system and analysed using LI-COR Image Studio LI-COR Biosciences.

Statistics. For plaque assay of virus replication data, p values were calculated using a paired, two-tailed Student's t-test. For differential gene and protein expression analysis, significant changes in specific genes or proteins (padj =< 0.05) were identified after adjusting for false discovery rate using the Benjamini Hochberg method. For gene ontology analysis, g:Profiler analysis was performed with the followed parameters (g:SCS threshold =< 0.05). For AP-MS, significant interactors were determined by two-tailed t-tests with permutation-based false discovery rate statistics. We performed 250 permutations, and the FDR threshold was set at 0.05. The parameter S0 was set to 1 to separate background from specifically enriched interactors. All statistical analyses were performed using R v4.3.0. The protein sequences of *R. microplus* UPF1 gene were compared and aligned with their respective homologues from other representative eukaryote species, including *Drosophila melanogaster*, *Daphnia pulex*, *I. scapularis*, *Apis melifera*, *Bombyx mori*, *Culex pipiens*, *Aedes aegypti*, *Mus musculus*, *Homo sapiens* and *Caenorhabditis elegans*. Multiple sequence alignments and phylogenetic analyses were conducted using MEGA6 software. The neighbour-joining method was employed to construct phylogenetic trees.

Data statement. The mass spectrometry-based proteomics data for both PIT and AP-MS have been deposited in the ProteomeXchange Consortium (http://proteomecentral.proteomexchange.org) via the PRIDE partner repository with the following dataset identifiers: PXDXXXX and PXD052311 Source data are provided with this paper. Transcriptomics data have been deposited in the NCBI repository under the following BioProject PRJNA1116706. Metadata related to other experiments including RT-qPCR and virus titration are available on https://doi.org/10.5525/gla.researchdata.1632.

Declarations

Funding information

This project received funding from the European Union's Horizon 2020 Research and Innovation Programme under the Marie Skłodowska-Curie grant agreement No 890970 (M.J.P.). Work was also supported by the UK Medical Research Council (MC_UU_12014/8 and MC_UU_00034/4) (A.K.), Wellcome Trust/Royal Society Sir Henry Dale Fellowship (210462/Z/18/Z) (B.B.), the UK Biotechnology and Biological Sciences Research Council (BB/P024270/1) (L.B.-S.), Q.G. was funded by UK Medical Research Council MC_UU_00034/5, the Wellcome Trust (223743/Z/21/Z) (L.B.-

S.), Free and Hanseatic City of Hamburg (P.S.), and Deutsche Forschungsgemeinschaft (DFG, German Research Foundation; project number SC 314/2-1) (P.S.).

Author contributions

M.J.P. - Conceptualization, Data Curation, Formal Analysis, Funding Acquisition, Investigation, Methodology, Software, Validation, Visualization, Writing – original draft, Writing – review & editing; C.F. - Formal Analysis, Investigation, Methodology, Resources, Validation, Visualization, Writing – original draft, Writing – review & editing; Q.G. - Formal Analysis, Investigation, Methodology, Software, Validation, Visualization, Writing – original draft, Writing – review & editing; M.F. - Investigation, Methodology, Writing – review & editing; D.L. - Investigation, Methodology, Writing – review & editing; A.S. - Investigation, Methodology, Writing – review & editing; K.D. - Investigation, Methodology, Writing – review & editing; L.B.-S. - Resources, Writing – review & editing; P.S. - Conceptualization, Data Curation, Funding Acquisition, Methodology, Project administration, Resources, Supervision, Writing – original draft, Writing – review & editing; B.B. - Conceptualization, Data Curation, Funding Acquisition, Methodology, Project administration, Resources, Supervision, Writing – original draft, Writing – review & editing; A.K. - Conceptualization, Data Curation, Funding Acquisition, Methodology, Project administration, Resources, Supervision, Writing – original draft, Writing – review & editing.

References

1. Yu, X.J. *et al.* Fever with thrombocytopenia associated with a novel bunyavirus in China. *N Engl J Med* **364**, 1523-1532 (2011).

2. Ren, Y.T. *et al.* Extensive genetic diversity of severe fever with thrombocytopenia syndrome virus circulating in Hubei Province, China, 2018-2022. *PLoS Negl Trop Dis* **17**, e0011654 (2023).

3. Seo, J.W., Kim, D., Yun, N. & Kim, D.M. Clinical Update of Severe Fever with Thrombocytopenia Syndrome. *Viruses* **13** (2021).

4. Kim, K.H. *et al.* Severe fever with thrombocytopenia syndrome, South Korea, 2012. *Emerg Infect Dis* **19**, 1892-1894 (2013).

5. Takahashi, T. *et al.* The first identification and retrospective study of Severe Fever with Thrombocytopenia Syndrome in Japan. *J Infect Dis* **209**, 816-827 (2014).

6. Lin, T.L. *et al.* The first discovery of severe fever with thrombocytopenia syndrome virus in Taiwan. *Emerg Microbes Infect* **9**, 148-151 (2020).

7. Tran, X.C. *et al.* Endemic Severe Fever with Thrombocytopenia Syndrome, Vietnam. *Emerg Infect Dis* **25**, 1029-1031 (2019).

8. Liu, B., Zhu, J., He, T. & Zhang, Z. Genetic variants of Dabie bandavirus: classification and biological/clinical implications. *Virol J* **20**, 68 (2023).

9. Yang, T., Huang, H., Jiang, L. & Li, J. Overview of the immunological mechanism underlying severe fever with thrombocytopenia syndrome (Review). *Int J Mol Med* **50** (2022).

10. Wang, M., Tan, W., Li, J., Fang, L. & Yue, M. The Endless Wars: Severe Fever With Thrombocytopenia Syndrome Virus, Host Immune and Genetic Factors. *Front Cell Infect Microbiol* **12**, 808098 (2022).

11. Wang, T., Xu, L., Zhu, B., Wang, J. & Zheng, X. Immune escape mechanisms of severe fever with thrombocytopenia syndrome virus. *Front Immunol* **13**, 937684 (2022).

12. Sun, Y., Li, J., Gao, G.F., Tien, P. & Liu, W. Bunyavirales ribonucleoproteins: the viral replication and transcription machinery. *Crit Rev Microbiol* **44**, 522-540 (2018).

13. Malet, H., Williams, H.M., Cusack, S. & Rosenthal, M. The mechanism of genome replication and transcription in bunyaviruses. *PLoS Pathog* **19**, e1011060 (2023).

14. Zhuang, L. *et al.* Transmission of Severe Fever with Thrombocytopenia Syndrome Virus by Haemaphysalis longicornis Ticks, China. *Emerg Infect Dis* **24**, 868-871 (2018).

15. Kim, H.G., Jung, M. & Lee, D.H. Seasonal activity of Haemaphysalis longicornis and Haemaphysalis flava (Acari: Ixodida), vectors of severe fever with thrombocytopenia syndrome (SFTS) virus, and their SFTS virus harboring rates in Gyeonggi Province, South Korea. *Exp Appl Acarol* **87**, 97-108 (2022).

16. Fares, M. & Brennan, B. Virus-host interactions during tick-borne bunyavirus infection. *Curr Opin Virol* **57**, 101278 (2022).

17. de la Fuente, J. *et al.* Tick-Pathogen Interactions and Vector Competence: Identification of Molecular Drivers for Tick-Borne Diseases. *Front Cell Infect Microbiol* **7**, 114 (2017).

18. Talactac, M.R. *et al.* The antiviral immunity of ticks against transmitted viral pathogens. *Dev Comp Immunol* **119**, 104012 (2021).

19. Schnettler, E. *et al.* Induction and suppression of tick cell antiviral RNAi responses by tick-borne flaviviruses. *Nucleic Acids Res* **42**, 9436-9446 (2014).

20. Weisheit, S. *et al.* Ixodes scapularis and Ixodes ricinus tick cell lines respond to infection with tick-borne encephalitis virus: transcriptomic and proteomic analysis. *Parasit Vectors* **8**, 599 (2015).

21. Grabowski, J.M., Gulia-Nuss, M., Kuhn, R.J. & Hill, C.A. RNAi reveals proteins for metabolism and protein processing associated with Langat virus infection in Ixodes scapularis (black-legged tick) ISE6 cells. *Parasit Vectors* **10**, 24 (2017).

22. McNally, K.L. *et al.* Differential salivary gland transcript expression profile in Ixodes scapularis nymphs upon feeding or flavivirus infection. *Ticks Tick Borne Dis* **3**, 18-26 (2012).

23. Mansfield, K.L. *et al.* Tick-borne pathogens induce differential expression of genes promoting cell survival and host resistance in Ixodes ricinus cells. *Parasit Vectors* **10**, 81 (2017).

24. Xu, Y. *et al.* Antiviral RNA interference in disease vector (Asian longhorned) ticks. *PLoS Pathog* **17**, e1010119 (2021).

25. Kim, Y.K. & Maquat, L.E. UPFront and center in RNA decay: UPF1 in nonsense-mediated mRNA decay and beyond. *RNA* **25**, 407-422 (2019).

26. Ullah, R., Li, J., Fang, P., Xiao, S. & Fang, L. DEAD/H-box helicases:Anti-viral and pro-viral roles during infections. *Virus Res* **309**, 198658 (2022).

27. Bell-Sakyi, L., Darby, A., Baylis, M. & Makepeace, B.L. The Tick Cell Biobank: A global resource for in vitro research on ticks, other arthropods and the pathogens they transmit. *Ticks Tick Borne Dis* **9**, 1364-1371 (2018).

28. Bell-Sakyi, L. Ehrlichia ruminantium grows in cell lines from four ixodid tick genera. *J Comp Pathol* **130**, 285-293 (2004).

29. Fauver, J.R. *et al.* A reverse-transcription/RNase H based protocol for depletion of mosquito ribosomal RNA facilitates viral intrahost evolution analysis, transcriptomics and pathogen discovery. *Virology* **528**, 181-197 (2019).

30. Grabherr, M.G. *et al.* Full-length transcriptome assembly from RNA-Seq data without a reference genome. *Nat Biotechnol* **29**, 644-652 (2011).

31. Altschul, S.F., Gish, W., Miller, W., Myers, E.W. & Lipman, D.J. Basic local alignment search tool. *J Mol Biol* **215**, 403-410 (1990).

32. Huerta-Cepas, J. *et al.* eggNOG 4.5: a hierarchical orthology framework with improved functional annotations for eukaryotic, prokaryotic and viral sequences. *Nucleic Acids Res* **44**, D286-293 (2016).

33. Kanehisa, M., Furumichi, M., Tanabe, M., Sato, Y. & Morishima, K. KEGG: new perspectives on genomes, pathways, diseases and drugs. *Nucleic Acids Res* **45**, D353-D361 (2017).

34. Jones, P. *et al.* InterProScan 5: genome-scale protein function classification. *Bioinformatics* **30**, 1236-1240 (2014).

35. Paysan-Lafosse, T. *et al.* InterPro in 2022. *Nucleic Acids Res* **51**, D418-D427 (2023).

36. Li, C.X. *et al.* Unprecedented genomic diversity of RNA viruses in arthropods reveals the ancestry of negative-sense RNA viruses. *Elife* **4** (2015).

37. Bell-Sakyi, L. & Attoui, H. Endogenous tick viruses and modulation of tick-borne pathogen growth. *Front Cell Infect Microbiol* **3**, 25 (2013).

38. Kholodilov, I.S. *et al.* Isolation and Characterisation of Alongshan Virus in Russia. *Viruses* **12** (2020).

39. Haas, B.J. *et al.* Automated eukaryotic gene structure annotation using EVidenceModeler and the Program to Assemble Spliced Alignments. *Genome Biol* **9**, R7 (2008).

40. Jia, N. *et al.* Large-Scale Comparative Analyses of Tick Genomes Elucidate Their Genetic Diversity and Vector Capacities. *Cell* **182**, 1328-1340 e1313 (2020).

41. Dobin, A. *et al.* STAR: ultrafast universal RNA-seq aligner. *Bioinformatics* **29**, 15-21 (2013).

42. Feng, C. *et al.* A novel eukaryotic RdRP-dependent small RNA pathway represses antiviral immunity by controlling an ERK pathway component in the black-legged tick. *bioRxiv*, 2021.2009.2019.460923 (2022).

43. Rosa, R.D. *et al.* Exploring the immune signalling pathway-related genes of the cattle tick Rhipicephalus microplus: From molecular characterization to transcriptional profile upon microbial challenge. *Dev Comp Immunol* **59**, 1-14 (2016).

44. O'Neal, A.J. *et al.* Croquemort elicits activation of the immune deficiency pathway in ticks. *Proc Natl Acad Sci U S A* **120**, e2208673120 (2023).

45. Merkling, S.H. *et al.* The heat shock response restricts virus infection in Drosophila. *Sci Rep* **5**, 12758 (2015).

46. Fogaca, A.C. *et al.* Tick Immune System: What Is Known, the Interconnections, the Gaps, and the Challenges. *Front Immunol* **12**, 628054 (2021).

47. Messmer, M. *et al.* DEAD box RNA helicase 5 is a new pro-viral host factor for Sindbis virus infection. *bioRxiv*, 2023.2009.2021.558232 (2024).

48. Nelson, C.R. *et al.* Human DDX17 Unwinds Rift Valley Fever Virus Non-Coding RNAs. *Int J Mol Sci* **22** (2020).

49. Rezelj, V.V. *et al.* Differential Antagonism of Human Innate Immune Responses by Tick-Borne Phlebovirus Nonstructural Proteins. *mSphere* **2** (2017).

50. Iranpour, M. *et al.* Apoptosis, autophagy and unfolded protein response pathways in Arbovirus replication and pathogenesis. *Expert Rev Mol Med* **18**, e1 (2016).

51. Causier, B. *et al.* Conservation of Nonsense-Mediated mRNA Decay Complex Components Throughout Eukaryotic Evolution. *Sci Rep-Uk* **7** (2017).

52. Mongelli, V. *et al.* Innate immune pathways act synergistically to constrain RNA virus evolution in Drosophila melanogaster. *Nat Ecol Evol* **6**, 565-578 (2022).

53. Fang, L.Z., Xiao, X., Lei, S.C., Liu, J.W. & Yu, X.J. Haemaphysalis flava ticks as a competent vector of severe fever with thrombocytopenia syndrome virus. *Ticks Tick Borne Dis* **14**, 102100 (2023).

54. Petit, M.J. & Shah, P.S. Mapping Arbovirus-Vector Interactions Using Systems Biology Techniques. *Front Cell Infect Microbiol* **8**, 440 (2018).

55. de la Fuente, J. *et al.* Tick Genome Assembled: New Opportunities for Research on Tick-Host-Pathogen Interactions. *Front Cell Infect Microbiol* **6**, 103 (2016).

56. Wang, G.Y. *et al.* Characterization and identification of long non-coding RNAs based on feature relationship. *Bioinformatics* **35**, 2949-2956 (2019).

57. Gaston, K.W. & Limbach, P.A. The identification and characterization of non-coding and coding RNAs and their modified nucleosides by mass spectrometry. *Rna Biol* **11**, 1568-1585 (2014).

58. Ahmad, P., Bensaoud, C., Mekki, I., Rehman, M.U. & Kotsyfakis, M. Long Non-Coding RNAs and Their Potential Roles in the Vector-Host-Pathogen Triad. *Life-Basel* **11** (2021).

59. Behnia, M. & Bradfute, S.B. The Host Non-Coding RNA Response to Alphavirus Infection. *Viruses* **15** (2023).

60. Madhry, D. *et al.* Role of non-coding RNAs in Dengue virus-host interaction. *Front Biosci (Schol Ed)* **13**, 44-55 (2021).

61. Miesen, P., Joosten, J. & van Rij, R.P. PIWIs Go Viral: Arbovirus-Derived piRNAs in Vector Mosquitoes. *PLoS Pathog* **12**, e1006017 (2016).

62. Grabowski, J.M. *et al.* Changes in the Proteome of Langat-Infected Ixodes scapularis ISE6 Cells: Metabolic Pathways Associated with Flavivirus Infection. *PLoS Negl Trop Dis* **10**, e0004180 (2016).

63. Heber, S. *et al.* Staufen2-mediated RNA recognition and localization requires combinatorial action of multiple domains. *Nat Commun* **10**, 1659 (2019).

64. Jin, J. *et al.* The cap-snatching frequency of a plant bunyavirus from nonsense mRNAs is low but is increased by silencing of UPF1 or SMG7. *Mol Plant Pathol* **23**, 576-582 (2022).

65. Mir, M.A., Duran, W.A., Hjelle, B.L., Ye, C. & Panganiban, A.T. Storage of cellular 5' mRNA caps in P bodies for viral cap-snatching. *Proc Natl Acad Sci U S A* **105**, 19294-19299 (2008).

66. Lee, T. & Pelletier, J. The biology of DHX9 and its potential as a therapeutic target. *Oncotarget* **7**, 42716-42739 (2016).

67. Brady, S. *et al.* Virion-associated, host-derived DHX9/RNA helicase A enhances the processivity of HIV-1 reverse transcriptase on genomic RNA. *J Biol Chem* **294**, 11473-11485 (2019).

68. Ren, X. *et al.* Nucleic DHX9 cooperates with STAT1 to transcribe interferon-stimulated genes. *Sci Adv* **9**, eadd5005 (2023).

69. Montavon, T.C. *et al.* Human DICER helicase domain recruits PKR and modulates its antiviral activity. *PLoS Pathog* **17**, e1009549 (2021).

70. Matkovic, R. *et al.* The Host DHX9 DExH-Box Helicase Is Recruited to Chikungunya Virus Replication Complexes for Optimal Genomic RNA Translation. *J Virol* **93** (2019).

71. Kudome, N. *et al.* The DEAD/H-box helicase DHX9 contributes to suppression of Bombyx mori nucleopolyhedrovirus propagation in B. mori cells. *Dev Comp Immunol* **147**, 104897 (2023).

72. Brennan, B. *et al.* Reverse genetics system for severe fever with thrombocytopenia syndrome virus. *J Virol* **89**, 3026-3037 (2015).

73. Chambers, M.C. *et al.* A cross-platform toolkit for mass spectrometry and proteomics. *Nat Biotechnol* **30**, 918-920 (2012).

74. Buchfink, B., Reuter, K. & Drost, H.G. Sensitive protein alignments at tree-of-life scale using DIAMOND. *Nat Methods* **18**, 366-368 (2021).

75. Haas, B.J. *et al.* Improving the Arabidopsis genome annotation using maximal transcript alignment assemblies. *Nucleic Acids Res* **31**, 5654-5666 (2003).

76. Stanke, M., Diekhans, M., Baertsch, R. & Haussler, D. Using native and syntenically mapped cDNA alignments to improve de novo gene finding. *Bioinformatics* **24**, 637-644 (2008).

77. Korf, I. Gene finding in novel genomes. *BMC Bioinformatics* **5**, 59 (2004).

78. Slater, G.S. & Birney, E. Automated generation of heuristics for biological sequence comparison. *Bmc Bioinformatics* **6** (2005).

79. Li, H. Protein-to-genome alignment with miniprot. *Bioinformatics* **39** (2023).

80. Gremme, G., Brendel, V., Sparks, M.E. & Kurtz, S. Engineering a software tool for gene structure prediction in higher organisms. *Inform Software Tech* **47**, 965-978 (2005).

81. Anders, S., Pyl, P.T. & Huber, W. HTSeq--a Python framework to work with high-throughput sequencing data. *Bioinformatics* **31**, 166-169 (2015).

82. Love, M.I., Huber, W. & Anders, S. Moderated estimation of fold change and dispersion for RNA-seq data with DESeq2. *Genome Biol* **15**, 550 (2014).

83. Zhu, A., Ibrahim, J.G. & Love, M.I. Heavy-tailed prior distributions for sequence count data: removing the noise and preserving large differences. *Bioinformatics* **35**, 2084-2092 (2019).

84. Raudvere, U. *et al.* g:Profiler: a web server for functional enrichment analysis and conversions of gene lists (2019 update). *Nucleic Acids Res* **47**, W191-W198 (2019).

85. Tyanova, S. *et al.* The Perseus computational platform for comprehensive analysis of (prote)omics data. *Nat Methods* **13**, 731-740 (2016).

86. Scaturro, P. *et al.* An orthogonal proteomic survey uncovers novel Zika virus host factors. *Nature* **561**, 253-257 (2018).

87. Wanner, N. *et al.* Molecular consequences of SARS-CoV-2 liver tropism. *Nat Metab* **4**, 310-319 (2022).

88. Tyanova, S., Temu, T. & Cox, J. The MaxQuant computational platform for mass spectrometry-based shotgun proteomics. *Nat Protoc* **11**, 2301-2319 (2016).

89. Shannon, P. *et al.* Cytoscape: a software environment for integrated models of biomolecular interaction networks. *Genome Res* **13**, 2498-2504 (2003).

90. Livak, K.J. & Schmittgen, T.D. Analysis of relative gene expression data using real-time quantitative PCR and the 2(-Delta Delta C(T)) Method. *Methods* **25**, 402-408 (2001).

91. Cao, J. *et al.* Severe fever with thrombocytopenia syndrome virus (SFTSV)-host interactome screen identifies viral nucleoprotein-associated host factors as potential antiviral targets. *Comput Struct Biotechnol J* **19**, 5568-5577 (2021).

Figures

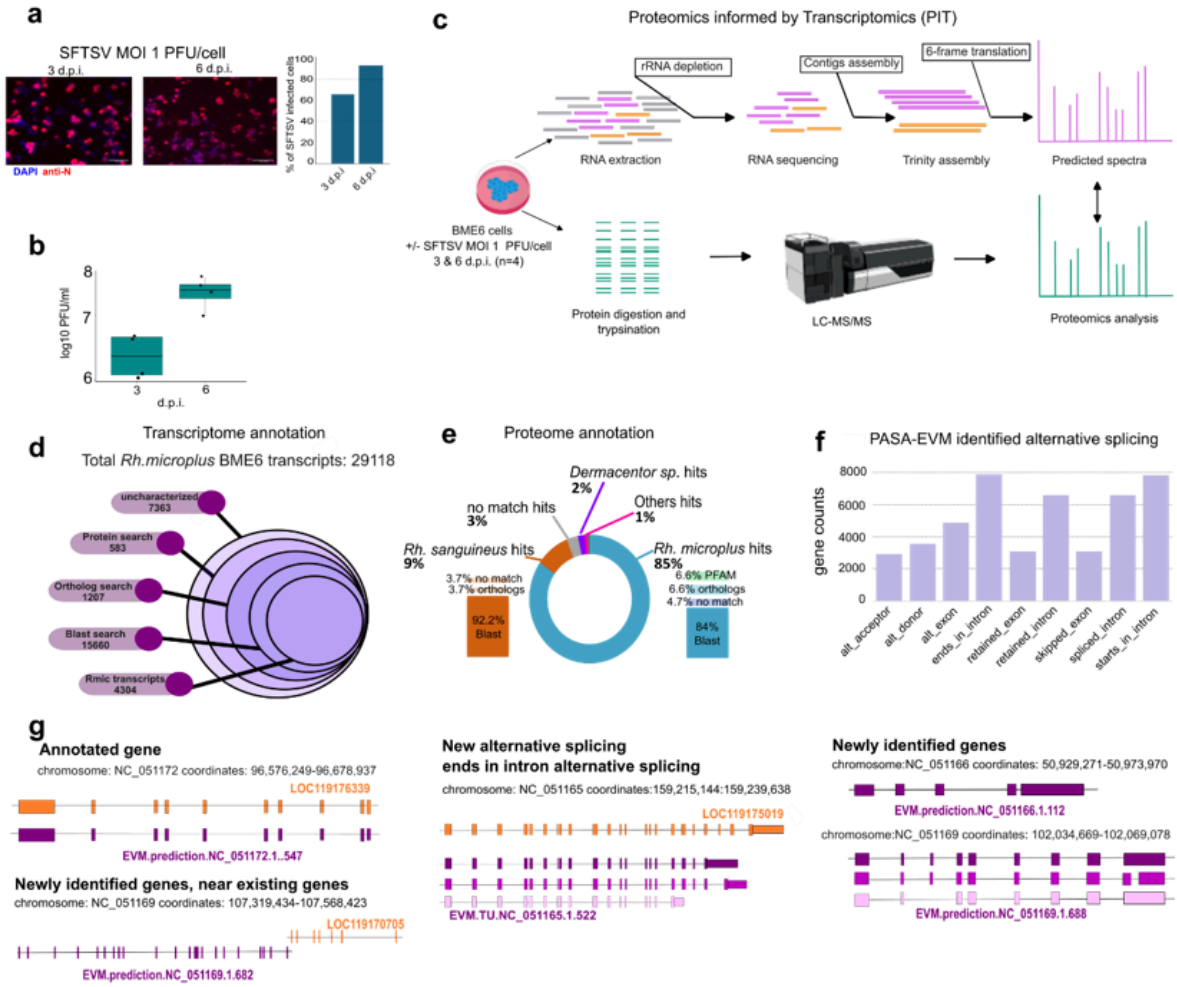

Figure 1

Proteomics informed by transcriptomics (PIT) methodology for *R. microplus* BME6 cells infected with SFTSV. BME6 cells were infected at MOI 1 PFU/cell and samples were collected at 3 and 6 d.p.i. **a.** Immunostaining of the SFTSV N protein (red) and DNA (blue) at 3 or 6 d.p.i. Bar graphs represent the percentage of SFTSV N (red) positive cells compared to DAPI positive cells (blue), n= 362 cells for 3 d.p.i. and n = 448 for 6 d.p.i.. **b.** Quantification of SFTSV titres by plaque assay (shown in Log_{10} PFU/ml), dots represent biological replicates (n=4). **c.** Schematic of the PIT experimental procedure designed for mock and SFTSV-infected BME6 cells. **d**. Annotation results for the *de novo* transcriptome; 29118 gene structures identified by PASA-EVM softwares, 6332 were identified by BLAST search on tick genome, 16,683 identified by ortholog search using EggNOG software and 583 identified by protein domain searches. Structure of 7883 genes did not yield a match (uncharacterized). **e.** Annotation results for the BME6 proteome, of 4750 proteins identified by PIT, 85% were identified as *R. microplus* (cyan) by BLAST, orthologs search (EggNOG), and protein domain identification (PFAM) as presented in the bar plot. 9 % were associated with *R. sanguineus* (brown), by BLAST search or ortholog search (EggNOG). Finally, 3% of the proteins did not yield a match (grey), 2% associated with *Dermacentor* species (purple), and 1% with other species (pink). **f.** Gene counts associated with newly identified alternative splicing events identified via the PASA-EVM pipeline. **g.** Examples of novel annotations or novel splicing events in the *R. microplus* genome. Boxes represents introns and line exons, orange gene structure associated with LOC ID refers to current RMIC18 genome annotation from Ensembl Metazoa. Dark purple gene structures represent newly PASA-EVM identified structures, light of purple structures represents isoforms. EVM ID was used to refer to the database. We selected examples to illustrate the novel annotations including gene that were identical (positive control); and example of novel annotation like alternative splicing (alternative ends, here); and finally new gene structures.

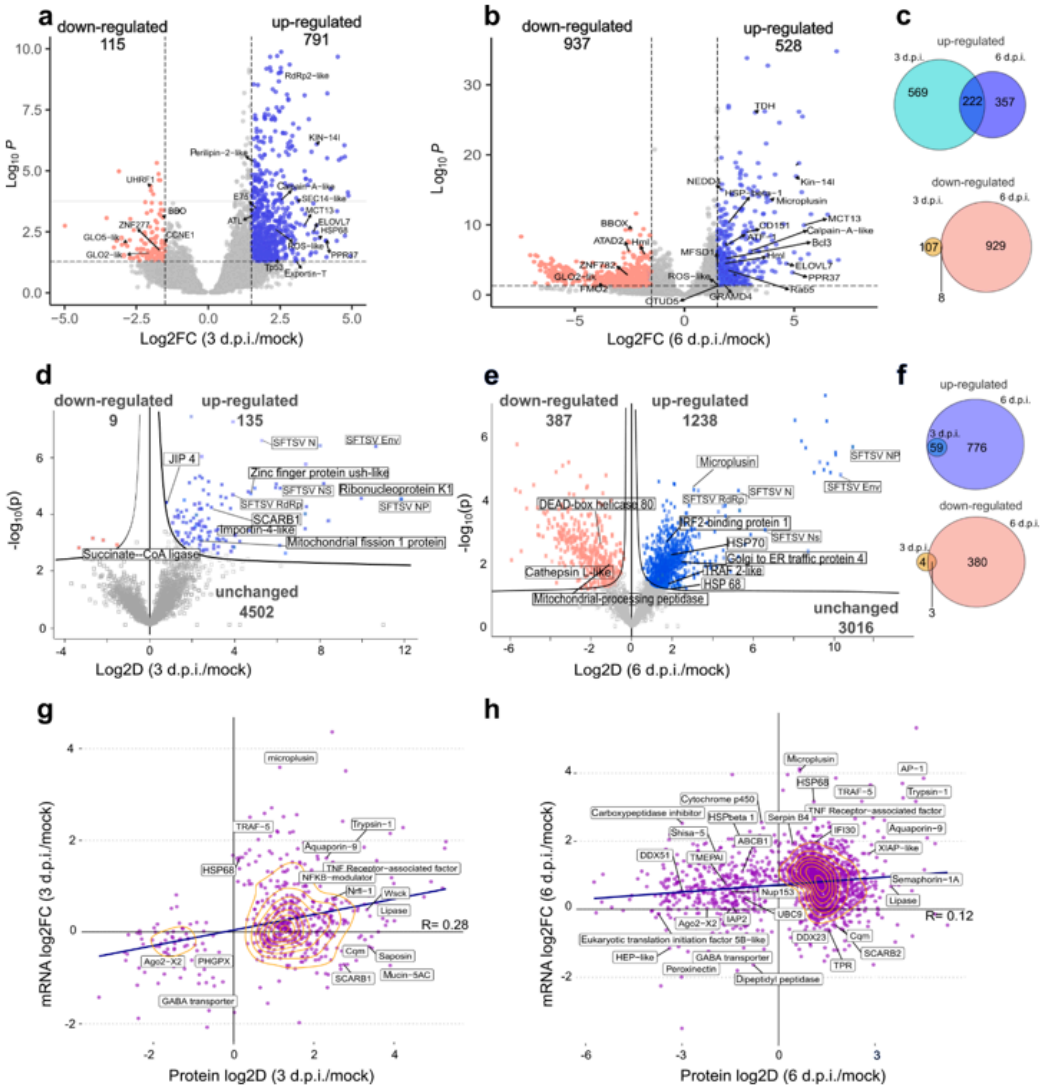

Figure 2

Differential transcript expression and protein levels in SFTSV-infected *R. microplus* BME6 cells. RNA and protein samples were prepared from mock or SFTSV-infected (MOI 1 PFU/cell) BME6 cells and analysed for mRNA expression and protein biosynthesis in response to infection. **a-b**. Differential RNA expression volcano plots. X axis represents the Log2 Fold Change (Log_2FC) when comparing 3 d.p.i **(a)** or 6 d.p.i **(b)** to mock-infected cells. The y axis shows Log_{10}(padj). Blue dots represent up-regulated transcripts, (Log_2FC>1.5, padj<0.05) and red dots down-regulated transcripts (log2FC<-1.5, padj<0.05). Gray dots represent non-significantly regulated RNAs (padj>0.05). **c.** Venn-diagram representing transcripts significantly differentially regulated (log2FC ± 1.5, padj<0.5) at 3 or 6 d.p.i., blue and red diagrams represent up- and down-regulation, respectively. **d-e**. Differential protein abundance volcano plot. X axis represents the Log_2 Difference (Log_2D) when comparing 3 d.p.i. **(d)** or 6 d.p.i. **(e)** to mock infected cells. The y axis shows -log_{10}(p). Blue dots represent significantly up-regulated (Log_2D>2, padj<0.05) proteins and red dots down-regulated proteins (Log_2D<-2, padj<0.05). Gray dots represent non-significantly regulated proteins (padj>0.05). **f**. Venn-diagram representing proteins significantly differentially regulated (Log_2FC ± 1.5, padj<0.5) at 3 and 6 d.p.i., blue and red diagrams represent up- and down-regulation, respectively. **g-h.** Scatter plot showing the correlation between protein (Y axis) and mRNA (X axis) expression ratios, Log_2D and Log_2FC, respectively. Purple dots represent genes and/or proteins with padj<0.5. k-means clusters are represented by yellow lines. **g**. Scatter plot showing differential expression of transcripts and proteins at 3 d.p.i. Pearson correlation factor of 0.28. **h.** Scatter plot for differential expression of transcripts and proteins at 6 d.p.i.. Pearson correlation factor of 0.12.

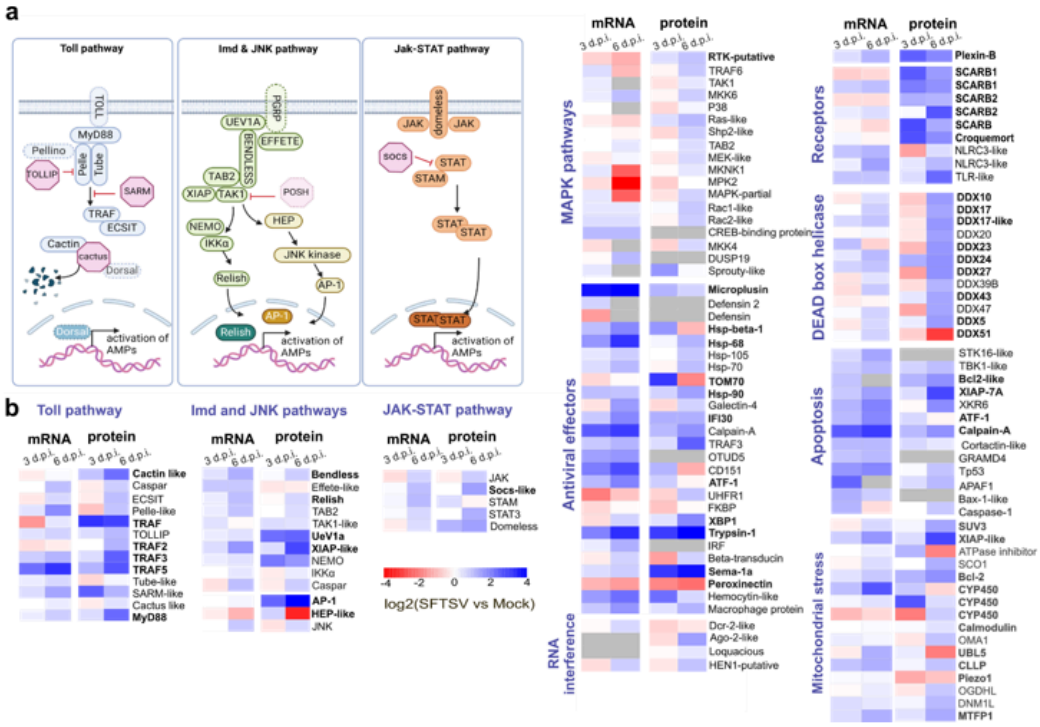

Figure 3

SFTSV differentially regulates core immune and stress pathways in infected *R. microplus* BME6 cells. **a.** Schematic representation of the core immune pathways Toll, Imd, JNK and JAK-STAT of BME6 cells. Dashed line represents a missing protein. **b.** Heat map showing the $\log_2$FC of transcripts and $\log_2$D of proteins from diverse pathways following SFTSV infection of BME6 cells. mRNA and protein expression were normalized to mock-infected BME6 cells. Expression levels of mRNA (left) and protein (right) were analysed at either 3 or 6 d.p.i.. Gray squares represent genes with no differential expression. Gene names in bold represent significantly differentially expressed genes and/or proteins.

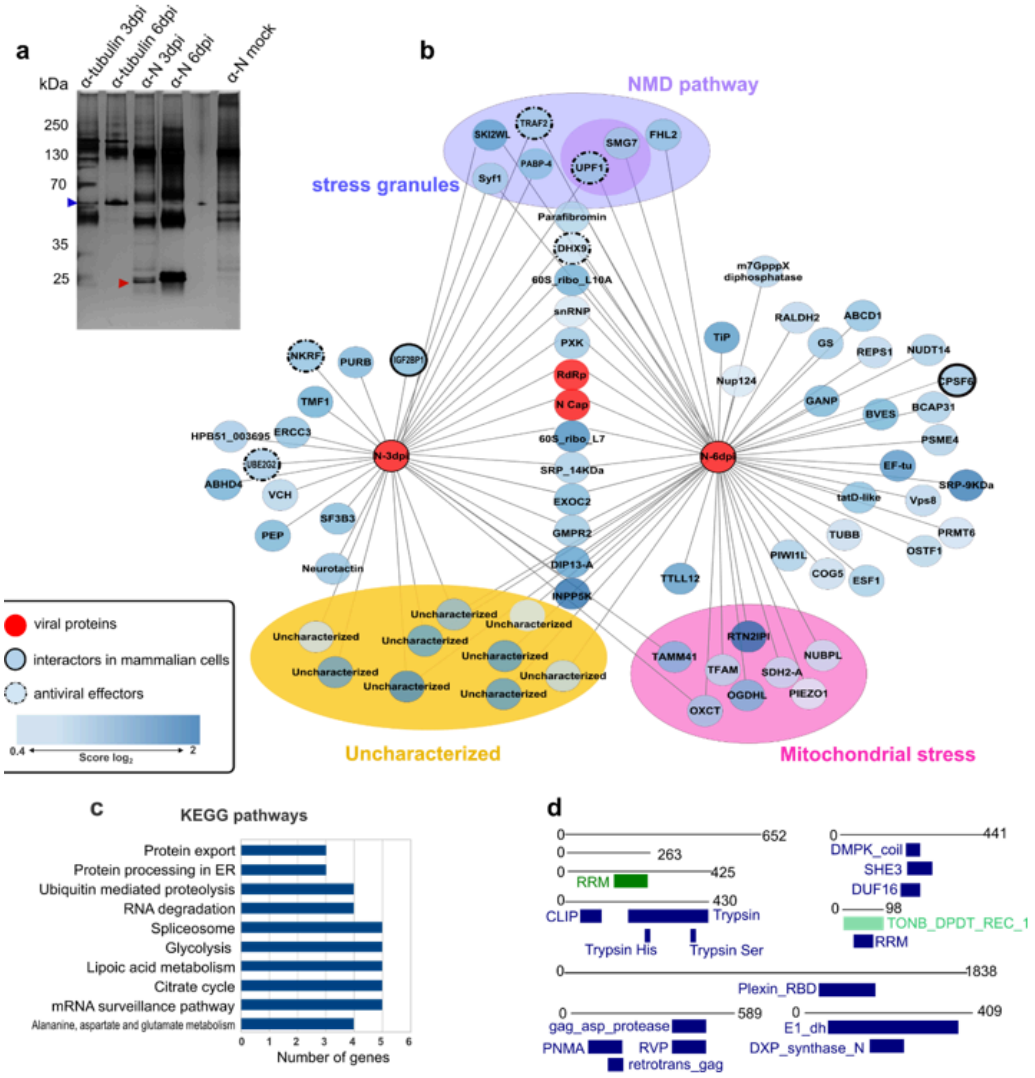

Figure 4

Network representation of the SFTSV N-*R. microplus* interactome in SFTSV-infected BME6 cells. a. Silver staining of mock or SFTSV-infected BME6 cell lysates following immunoprecipitation. Samples were immunoprecipitated with anti-tubulin as control (blue arrow) or SFTSV nucleocapsid protein N (red arrow). **b.** SFTSV N protein-protein interaction networks at 3 or 6 d.p.i., protein abbreviations/names were determined using the EggNOG ortholog search. Red dots indicate SFTSV proteins, bold black line highlights identified interactors of SFTSV-N protein in human cells [91], and dashed line represents proteins with previously demonstrated antiviral function. Yellow subgroup represents uncharacterized proteins, purple sub-group are proteins related to stress granules and non-sense mRNA decay pathway (NMD) while pink sub-group are proteins related to mitochondrial stress. Data shown from n=4 independent biological replicates. **c**. KEGG pathway analysis combining all interactors of SFTSV-N proteins. **d.** Uncharacterized protein sequences were searched for PFAM protein domains (MOTIF Search). Identified domains with $p<0.05$ are represented (Sup. Table 5). RRM= RNA recognition motif; DMPK_coil= myotonic dystrophy protein kinase coil; SHE3= SWI5-dependent HO expression protein 3; DUF16= domain of unknown function; Plexin_RBD= RhoGTPase-binding domain; PNMA= paraneoplastic antigens Ma-like; RVP= retroviral protease-like; E1_dh= dehydrogenase E1 component; DXP_synthase_N= 1-deoxy-D-xylulose-5-phosphate synthase.

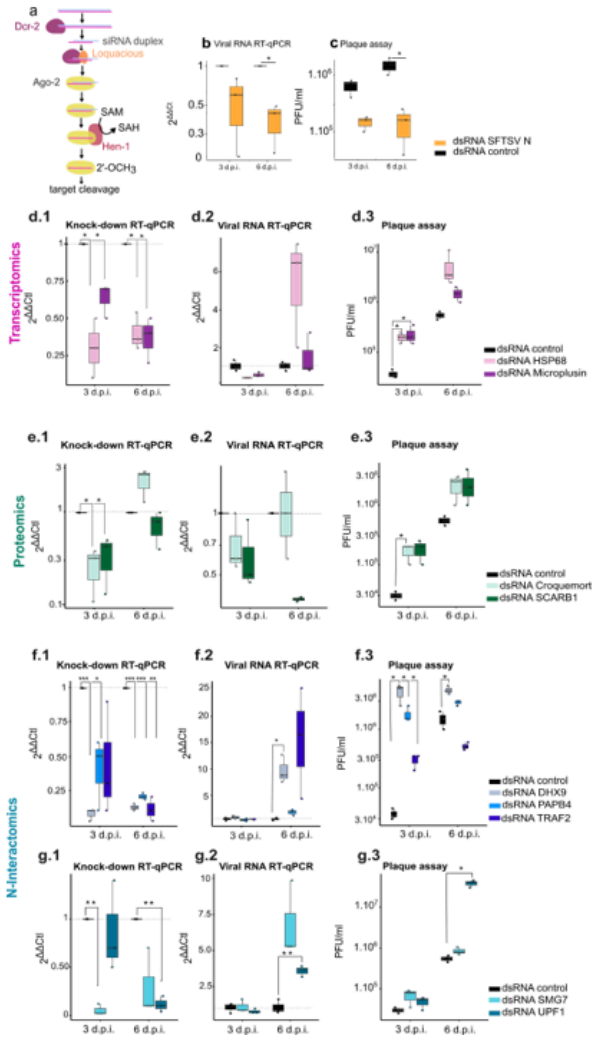

Figure 5

Gene silencing in *R. microplus* BME6 cells. a. siRNA pathway schematic. **b-c**. Cells were transfected using the Magnetofection O2 (OZ bioscience) with SFTSV N dsRNA or a control dsRNA (targeting *Renilla* luciferase) for 18 h prior to SFTSV infection at MOI 0.5 PFU/cell. **b.** Quantification of SFTSV M segment by RT-qPCR at 3 and 6 d.p.i. RT-qPCR fold change was calculated using the housekeeping gene eiF1A using the $2^{\Delta\Delta CT}$ method. **c.** Quantification of SFTSV viral titres by plaque assay at 3 and 6 d.p.i.. **d-g.** Panels show dsRNA knock-down efficiency (**d.1-g.1**), SFTSV RNA quantification (**d.2-g.2**), and SFTSV titres as determined by plaque assay (**d.3-g.3**). For RT-qPCR fold change was calculated using the housekeeping gene eiF1A using the $2^{\Delta\Delta CT}$ method. **b-g**. Data from three independent biological replicates were plotted as mean values with standard deviation. P values were calculated using a paired, two-tailed Student's t-test. p-values are * p-value <= 0.05, ** p-value <= 0.01, *** p-value <= 0.001.